PHYSICAL REVIEW D **71,** 114012 (2005)

$\Lambda(1520, 3/2^-)$-photoproduction reaction via $\gamma N \to K\Lambda^*(1520)$

Seung-Il Nam*
Research Center for Nuclear Physics (RCNP), Osaka University, Ibaraki, Osaka 567-0047, Japan
Department of Physics and Nuclear Physics & Radiation Technology Institute (NuRI), Pusan National University, Busan 609-735, Republic of Korea

Atsushi Hosaka†
Research Center for Nuclear Physics (RCNP), Osaka University, Ibaraki, Osaka 567-0047, Japan

Hyun-Chul Kim‡
Department of Physics and Nuclear Physics & Radiation Technology Institute (NuRI), Pusan National University, Busan 609-735, Republic of Korea
(Received 14 April 2005; published 27 June 2005)

We investigate $\Lambda(1520, 3/2^-, D_{03})$ photoproduction via the $\gamma N \to K\Lambda^*$ process. Using effective Lagrangians, we compute the total and differential cross sections. The dependence on the momentum transfer for the photoproduction at the tree-level is also examined. We find that the total cross sections for the proton target are well reproduced as compared with the experimental data. It turns out that the total cross sections for the neutron target are significantly smaller than those for the proton one. We also compare the present results with the $\gamma N \to \bar{K}\Theta^+$ reaction in order to extract information of Θ^+. The role of K^*-exchange in the production reaction is also discussed.

DOI: 10.1103/PhysRevD.71.114012 PACS numbers: 13.75.Cs, 14.20.−c

I. INTRODUCTION

Recent interest in excited baryons has been largely motivated by new experimental developments [1]: The observation of the exotic Θ^+ resonance of strangeness $S = +1$ has triggered diverse activities in both experimental and theoretical studies. The finding of the Θ^+ has renewed interest in baryon spectroscopy. For instance, properties of the $\Lambda(1405)$ has been reanalyzed, based on the idea of chiral perturbation theory and of dynamical generation from (anti) kaon-nucleon scattering. A meson-baryon bound-state picture suggests another type of the multiquark structure. A spin-$3/2^-$ partner of this resonance, i.e. $\Lambda(1520)$ ($\equiv \Lambda^*$) whose mass is similar to that of Θ^+ but strangeness is opposite is yet another interesting resonance. It can be produced simultaneously in the Θ^+ photoproduction from the deuteron target. The LEPS collaboration is searching for the Θ^+ associated with the production of the Λ^* in photoproduction off the deuteron [2]. Since the measurement of the Λ^* can be performed much more reliably, the detailed understanding of the production mechanism of this resonance would be useful to extract information of the Θ^+.

As far as the experimental data of the Λ^* production are concerned, there are experiments reported so far: Boyarski (photoproduction)*et al.* [3], the Daresbury group (photoproduction) [4], and the CLAS collaboration (electroproduction) [5]. However, these two production mechanisms showed rather different tendencies: While in Ref. [3] and in the Daresbury experiment K^*-exchange is known to be dominant in the t-channel, the CLAS experiment indicates that pseudoscalar K-exchange governs the process. Moreover, the kinematical regions of these experiments are different, so that a mere comparison is not meaningful.

In the present work, we investigate the photoproduction of the Λ^* near the threshold. Based on the effective Lagrangian for meson-baryon vertices, we use the Born approximation. We introduce form factors at the vertices, which reflect the internal structure of hadrons but bring in model dependence. However, there is a caveat: Introducing the form factors violates the gauge invariance of the electromagnetic interaction, which causes the Ward-Takahashi identity to be broken. Thus, we have to take care of the form factors to restore the gauge invariance. Since there is no unique theoretical way to introduce the gauge-invariant form factors, we shall adopt the prescriptions discussed in Refs. [6–8].

In the present approach, we treat the Λ^* with spin $J = 3/2$ in the Rarita-Schwinger formalism [9–16]. Since we consider the production of the real Λ^*, the uncertainty of the off-shell parameter in the Rarita-Schwinger parameterization can be minimized. In the present calculation, we consider both K- and K^*-exchanges in the t-channel. They show very different behaviors for spin-dependent quantities, which will be useful to study the mechanism of the photoproduction. Unknown parameters such as strong coupling constants and magnetic moments of the Λ^* will be adjusted so as to reproduce experimental data, being guided by the quark model. We shall consider the photoreactions for both proton and neutron targets in order to study the role of the isospin in understanding the reaction mechanism.

*Electronic address: sinam@rcnp.osaka-u.ac.jp
†Electronic address: hosaka@rcnp.osaka-u.ac.jp
‡Electronic address: hchkim@pusan.ac.kr

The outline of the paper is as follows: In Sec. II, we describe the effective Lagrangians for various meson-baryon vertices and construct the invariant amplitudes. In Sec. III, we demonstrate numerical results for total and differential cross sections both for the proton and neutron targets. Theoretical predictions are then compared with the existing experimental data. In the final Section, we will summarize the present work with some discussions.

II. GENERAL FORMALISM

We begin with the effective Lagrangians relevant to the $\gamma N \to K\Lambda^*$ process as depicted in Fig. 1. We define the momenta of photon, pseudoscalar kaon K, vector meson K^*, nucleon and Λ^* in the figure. For convenience, vector K^*-exchange in the t-channel and contact diagrams will be called as the υ-channel (vector channel) and c-channel (contact-term channel), respectively. We need to consider all diagrams shown in Fig. 1 for the proton target, whereas only the magnetic term in the s-channel, K^*-exchange in the υ and u-channels are required for the neutron target. In order to formulate the effective Lagrangians including spin-3/2 particles, we employ the Rarita-Schwinger (RS) field which we summarize in the Appendix.

The relevant effective Lagrangians are given as :

$$\begin{aligned}
&\mathcal{L}_{\gamma NN} = -e\bar{N}\left(\gamma_\mu + i\frac{\kappa_N}{2M_N}\sigma_{\mu\nu}k_1^\nu\right)A^\mu N + \text{h.c.}, \qquad \mathcal{L}_{\gamma KK} = ie\{(\partial^\mu K^\dagger)K - (\partial^\mu K)K^\dagger\}A_\mu, \\
&\mathcal{L}_{\gamma\Lambda^*\Lambda^*} = -\bar{\Lambda}^{*\mu}\left\{\left(-F_1\not{A}g_{\mu\nu} + F_3\not{A}\frac{k_{1\mu}k_{1\nu}}{2M_{\Lambda^*}^2}\right) - \frac{\not{k}_1\not{A}}{2M_{\Lambda^*}}\left(-F_2 g_{\mu\nu} + F_4\frac{k_{1\mu}k_{1\nu}}{2M_{\Lambda^*}^2}\right)\right\}\Lambda^{*\nu} + \text{h.c.}, \\
&\mathcal{L}_{\gamma KK^*} = g_{\gamma KK^*}\epsilon_{\mu\nu\sigma\rho}(\partial^\mu A^\nu)(\partial^\sigma K)K^{*\rho} + \text{h.c.}, \qquad \mathcal{L}_{KN\Lambda^*} = \frac{g_{KN\Lambda^*}}{M_K}\bar{\Lambda}^{*\mu}\Theta_{\mu\nu}(A,Z)(\partial^\nu K)\gamma_5 N + \text{h.c.}, \\
&\mathcal{L}_{K^*N\Lambda^*} = -\frac{ig_{K^*N\Lambda^*}}{M_{K^*}}\bar{\Lambda}^{*\mu}\gamma^\nu(\partial_\mu K_\nu^* - \partial_\nu K_\mu^*)N + \text{h.c.}, \qquad \mathcal{L}_{\gamma KN\Lambda^*} = -i\frac{eg_{KN\Lambda^*}}{M_K}\bar{\Lambda}^{*\mu}A_\mu K\gamma_5 N + \text{h.c.},
\end{aligned} \tag{1}$$

where N, Λ_μ^*, K and A^μ denote the nucleon, Λ^*, pseudoscalar kaon and photon fields, respectively. The interaction for the $K^*N\Lambda^*$ vertex is taken from Ref. [17]. As for the $\gamma\Lambda^*\Lambda^*$ vertex in the u-channel, we utilize the effective interaction suggested by Ref. [18] which contains four form factors of different multipoles. We ignore the electric coupling F_1, since the Λ^* is neutral. We also neglect F_3 and F_4 terms, assuming that higher multipole terms are less important. Hence, for the photon coupling to Λ^*, we consider only the magnetic coupling term F_2 whose strength is proportional to the anomalous magnetic moment of the Λ^*, i.e. κ_{Λ^*} which is treated as a free parameter. The off-shell term $\Theta_{\mu\nu}(A,Z)$ of the spin-3/2 particle is defined in general as follows [15,16]:

$$\Theta_{\mu\nu}(A,Z) = g_{\mu\nu} + \left\{\frac{1}{2}(1+4Z)A + Z\right\}\gamma_\mu\gamma_\nu. \tag{2}$$

If we choose $A = -1$ [10,15,16], we can rewrite Eq. (2) in the following form with a new parameter $X = -(Z + 1/2)$:

$$\Theta_{\mu\nu}(X) = g_{\mu\nu} + X\gamma_\mu\gamma_\nu, \tag{3}$$

where X is regarded as a free parameter in the present work.

In order to determine the coupling constant $g_{KN\Lambda^*}$, we make use of the full width $\Gamma_\Lambda = 15.6$ MeV and the branching ratio 0.45 for the decay $\Lambda^* \to \bar{K}N$ [19]. The coupling constant $KN\Lambda^*$ can be obtained by the following relation :

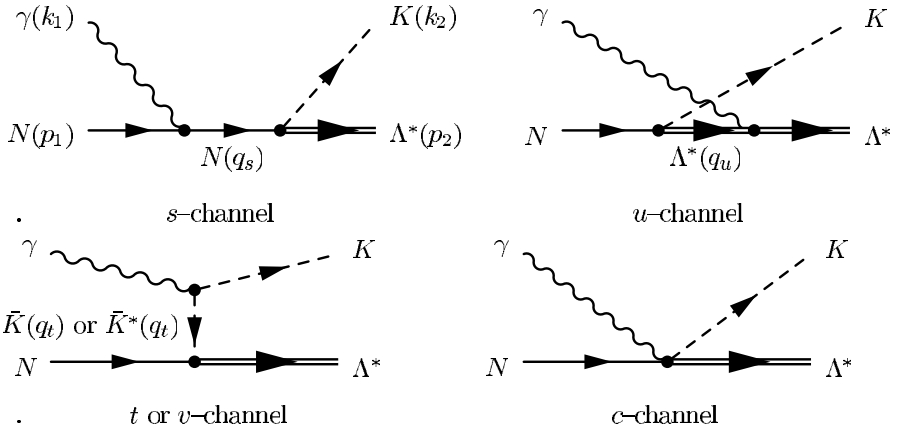

FIG. 1. The Feynmann diagrams

$$g_{KN\Lambda^*} = \left\{\frac{P_3}{4\pi M_{\Lambda^*}^2 M_K^2 \Gamma_{\Lambda^*}}\left(\frac{1}{4}\sum_{\text{spin}}|\mathcal{M}'|^2\right)\right\}^{-1/2},$$
$$i\mathcal{M}' = \bar{u}(P_2)\gamma_5 P_3^\mu u_\mu(P_1), \tag{4}$$

where P_1, P_2 and P_3 stand for the momenta of Λ^*, N and $\bar{K}$, respectively, for the two-body decay $\Lambda^* \to \bar{K}N$ in the center of mass frame. Thus, we obtain $g_{KN\Lambda^*} \sim 11$. As for the $K^*N\Lambda^*$ coupling constant, we will choose the values of $|g_{K^*N\Lambda^*}| = 0$ and $|g_{K^*N\Lambda^*}| = 11$ for the numerical calculation. In the nonrelativistic quark model, if Λ^* is described as a p-wave excitation of flavor-singlet spin-3/2 state, it is shown that the strength of the $K^*N\Lambda^*$ coupling constant is of the same order as that of $KN\Lambda^*$ or even larger than that. The coupling constant of the $g_{\gamma K^* K}$ is taken to be $0.254[\text{GeV}^{-1}]$ for the charged decay and $0.388[\text{GeV}^{-1}]$ for the neutral decay [19].

Taking all of these into consideration, we construct the invariant amplitudes as follows :

$$\begin{aligned}
i\mathcal{M}_s &= -\frac{e g_{KN\Lambda^*}}{M_K}\bar{u}^\mu(p_2, s_2)k_{2\mu}\gamma_5\frac{(\not{p}_1 + M_p)F_{1,c} + \not{k}_1 F_{1,s}}{q_s^2 - M_p^2}\not{\epsilon}u(p_1, s_1), \\
&\quad + \frac{e\kappa_p g_{KN\Lambda^*}}{2M_p M_K}\bar{u}^\mu(p_2, s_2)k_{2\mu}\gamma_5\frac{(\not{q}_s + M_p)F_{1,s}}{q_s^2 - M_p^2}\not{\epsilon}\not{k}_1 u(p_1, s_1) \\
i\mathcal{M}_u &= -\frac{g_{KN\lambda}\kappa_{\Lambda^*}}{2M_K M_\Lambda}\bar{u}_\mu(p_2)\not{k}_1\not{\epsilon}D_\sigma^\mu\Theta^{\sigma\rho}k_{2\rho}\gamma_5 u(p_1)F_{1,u}, \qquad \mathcal{M}_t = \frac{2e g_{KN\Lambda^*}}{M_K}\bar{u}^\mu(p_2, s_2)\frac{q_{t,\mu}k_2\cdot\epsilon}{q_t^2 - M_K^2}\gamma_5 u(p_1, s_1)F_{1,c}, \\
i\mathcal{M}_c &= \frac{e g_{KN\Lambda^*}}{M_K}\bar{u}^\mu(p_2, s_2)\epsilon_\mu\gamma_5 u(p_1, s_1)F_{1,c}, \\
i\mathcal{M}_\upsilon &= \frac{-ig_{\gamma KK^*}g_{K^*NB}}{M_{K^*}(q_t^2 - M_{K^*}^2)}\bar{u}^\mu(p_2, s_2)\gamma_\nu(q_t^\mu g^{\nu\sigma} - g_t^\nu q^{\mu\sigma})\epsilon_{\rho\eta\xi\sigma}k_1^\rho\epsilon^\eta k_2^\xi u(p_1, s_1)F_{1,\upsilon},
\end{aligned} \tag{5}$$

where ϵ^μ and u^μ are the photon polarization vector and the RS vector-spinor which is defined as follows:

$$u^\mu(p_2, s_2) = \sum_{\lambda,s}\left\langle 1\lambda\frac{1}{2}s|\frac{3}{2}s_2\right\rangle e^\mu(p_2, \lambda)u(p_2, s) \tag{6}$$

with the Clebsch-Gordan coefficient $\langle 1\lambda\frac{1}{2}s|\frac{3}{2}s_2\rangle$. $D_{\mu\nu}$ stands for the spin-3/2 propagator:

$$D_{\mu\nu} = -\frac{\not{q} + M_{\Lambda^*}}{q^2 - M_{\Lambda^*}^2}\left[g_{\mu\nu} - \frac{1}{3}\gamma_\mu\gamma_\nu - \frac{2}{3M_{\Lambda^*}^2}q_\mu q_\nu + \frac{q_\mu\gamma_\nu + q_\mu\gamma_\nu}{3M_{\Lambda^*}}\right]. \tag{7}$$

In Eq. (5), we have shown how the four-dimensional form factor is inserted in such way that gauge-invariance is preserved. As suggested in Ref. [7,8], we adopt the following parameterization for the four-dimensional form factors:

$$F_{1,x}(q^2) = \frac{\Lambda_1^4}{\Lambda_1^4 + (x - M_x^2)^2}, x = s, t, u, \upsilon$$
$$F_{1,c} = F_{1,s} + F_{1,t} - F_{1,s}F_{1,t}. \tag{8}$$

The form of $F_{1,c}$ is chosen such that the on-shell values of the coupling constants are reproduced.

We consider another type of the form factor with the three-momentum cutoff, which is parameterized as follows:

$$F_2(|\vec{k}_1|, |\vec{k}_2|) = \left(\frac{\Lambda_2^2}{\Lambda_2^2 + |\vec{k}_1|^2}\right)\left(\frac{\Lambda_2^2 - P_{KN\Lambda^*}^2}{\Lambda_2^2 + |\vec{k}_2|^2}\right), \tag{9}$$

where k_1 and k_2 denote the momenta of the initial photon and final kaon, respectively. We will multiply all the amplitudes $\mathcal{M}_{s,t,u,c,\upsilon}$ by the form factor F_2 to maintain gauge-invariance. In order to satisfy the normalization condition for the $KN\Lambda^*$ vertex, we set $P_{KN\Lambda^*} = 238$ MeV, considering the decay process $\Lambda^* \to \bar{K}N$. The cutoff masses Λ_1 and Λ_2 will be adjusted to produce the data of the total cross section $\sigma_{\gamma p\to K^+\Lambda^*}$.

III. NUMERICAL RESULTS

A. $\gamma N \to K\Lambda^*$ without the form factors

We first consider the numerical results for the total cross section of the $\gamma N \to K\Lambda^*$ process without form factors to examine the contributions of various channels which are depicted as functions of the incident photon energy E_γ in Fig. 2. Here, we choose the unknown parameters as follows: $\kappa_{\Lambda^*} = 1.0$, $X = 1$ and $g_{K^*N\Lambda^*} = g_{KN\Lambda^*} = +11$. The parameter dependence will be discussed later. The contact term, i.e. c-channel is dominant over all other channels for the proton target, as shown in the left panel of Fig. 2. Near the threshold, in particular, the c-and υ-channels are characterized by the energy dependence of the s-wave type, i.e. $\sigma \sim (E_\gamma - E_{\text{th}})^{1/2}$, where E_{th} stands for the threshold energy, although the magnitude of the υ-channel is much smaller than that of the c-channel. On the other hand, the s-, u-, and t-channels are governed by the p-wave, due to which their contributions turn out to be much smaller than those of the c-, and υ-ones in the vicinity of the threshold.

In the case of the neutron target, as depicted in the right panel of Fig. 2, the contact term is absent, which makes the $s-$channel the largest. Moreover, we also find a destructive

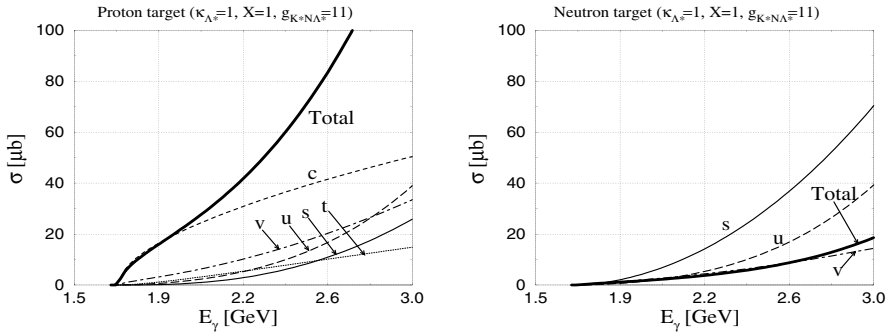

FIG. 2. Each contribution of various channels to the total cross sections without form factors. In the left panel, the total cross section for the proton target is depicted, while in the right panel that for the neutron one is drawn. We choose the parameters as follows: $(\kappa_{\Lambda^*}, X) = (1, 1)$ and $g_{KN\Lambda^*} = +11$.

interference between the s-, u- and v-channels, so that the total cross section for the neutron target turns out to be much smaller than that for the proton one. Although it is not shown here, we verified that forward scattering is enhanced both in the proton and neutron targets when the form factors are turned off.

B. $\gamma N \to K\Lambda^*$ with the form factor F_1

We are now in a position to introduce the form factor F_1 defined as in Eq. (8). In Fig. 3, the $s-$, t- and c-channel contributions to the total cross section for the proton target are drawn, separately. Note that they do not contain the parameters such as κ_{Λ^*}, X and $g_{K^*N\Lambda^*}$. The experimental data are taken from Ref. [4] in the range of the photon energy: 2.8 GeV $< E_\gamma <$ 4.8 GeV. The cutoff parameter is fixed to reproduce the experimental data. $\Lambda_1 = 750$ MeV is our best value. However, the results at higher energies should be taken cautiously, since the Born approximation is reliable only in the low-energy region near the threshold. In fact, we have found that the total cross section depends much on the parameters such as κ_{Λ^*} and X beyond $E_\gamma \gtrsim 3$ GeV, whereas it turns out that its dependence on those parameters is rather weak when $E_\gamma \lesssim 3$ GeV [20]. Therefore, we focus most of our discussion below $E_\gamma \lesssim 3$ GeV, where the Born approximation is expected to be reliable. It is interesting to observe that the size and

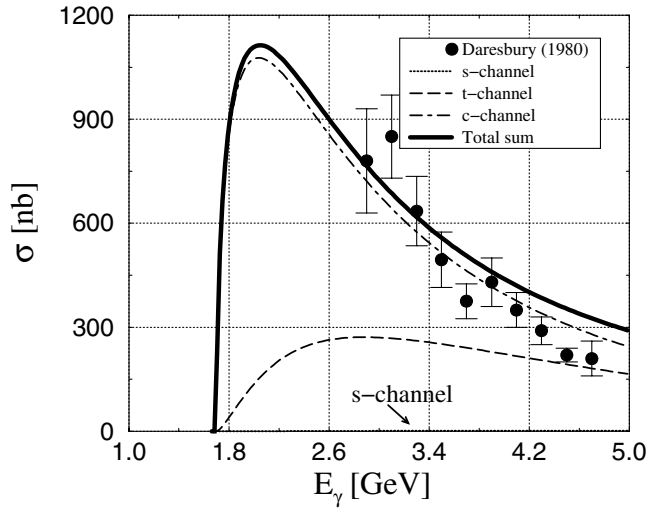

FIG. 3. The total cross sections for the proton target with the form factor F_1. The s-, t- and c-channel contributions are drawn separately. The experimental data are taken from Ref. [4]

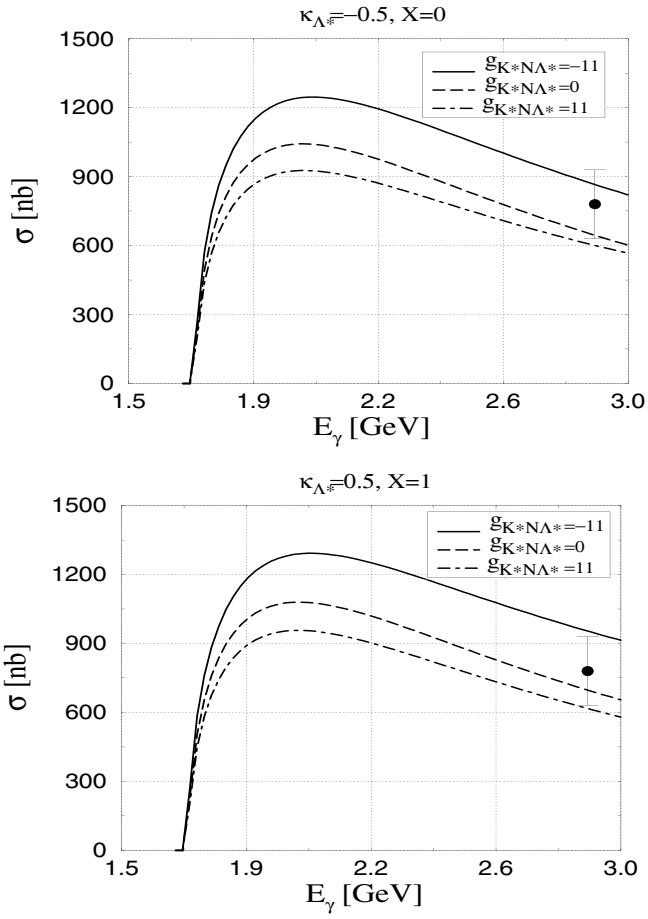

FIG. 4. The total cross sections for the proton target with the form factor F_1. We choose $(\kappa_{\Lambda^*}, X) = (-0.5, 0)$ and $(0.5, 1)$ in order to see the parameter dependence. We choose three different values of the coupling constant $g_{K^*N\Lambda^*} = 0$ and ± 11.

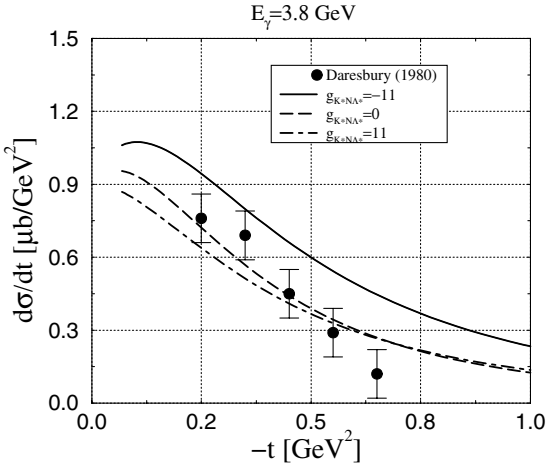

FIG. 5. The t-dependence for the proton target at $E_\gamma = 3.8$ GeV. We choose $(\kappa_{\Lambda^*}, X) = (0, 0)$. The experimental data are taken from Ref. [4]

energy dependence of the total cross section of the $\Lambda^*(1520)$ production are similar to those of the production of the ground state $\Lambda(1116)$ [3,4].

As shown in Fig. 3, the c-channel is the most dominant contribution without which one can never reproduce the data for the proton target. On the other hand, the s-channel contribution is almost negligible and the t-channel is marginal.

Figure 4 depicts the total cross sections with the coupling constant $g_{K^*N\Lambda^*}$ varied. We basically use the relation $g_{K^*N\Lambda^*} = \pm|g_{KN\Lambda^*}|$, i.e. $g_{K^*N\Lambda^*} = \pm 11$. The total cross sections are rather insensitive to its values.

These two results are also compared for the two different parameter sets, i.e. $(\kappa_{\Lambda^*}, X) = (-0.5, 0)$ and $(0.5, 1)$. As discussed previously, the results do not depend much on these parameters at $E_\gamma \lesssim 3$ GeV. In the quark model, it is found that the anomalous magnetic moment κ_{Λ^*} turns out to vanish in pure $SU(3)$ symmetry. Taking into account explicit $SU(3)$ symmetry breaking, we expect that the values of κ_{Λ^*} may lie in the range of $|\kappa_{\Lambda^*}| < 0.5$. However, we find from Fig. 4 that the dependence on κ_{Λ^*} within this range is rather small. Therefore, these two parameters κ_{Λ^*} and X can be safely set to be zero, i.e. $\kappa_{\Lambda^*} = X = 0$.

In Fig. 5, we depict the dependence on the momentum transfer, $d\sigma/dt$ (t-dependence) at $E_\gamma = 3.8$ GeV which is the average energy of the Daresbury experiment ($2.8 < E_\gamma < 4.8$ GeV) [4]. The figure indicates that the present work is in good agreement with the data. In Fig. 6, we also demonstrate the angular dependence. Here, θ is the angle between the incident photon and the outgoing kaon in the center of mass system. Each panel draws the differential cross sections $d\sigma/d(\cos\theta)$ with $g_{K^*N\Lambda^*}$ varied. We observe that K^*-exchange does not contribute much to the differential cross sections as in the case of the total cross sections (see also Fig. 4).

Figure 7 predicts the total cross section for the neutron target and $d\sigma/dt$ at $E_\gamma = 3.8$ GeV with the form factor F_1 being employed. In this case, the contact term is absent, since the process $\gamma n \to K^0\Lambda^*$ is the neutral one (see Eq. (5)). Its absence causes the total cross section to become much smaller than that for the proton target. The left panel of Fig. 7 depicts the total cross sections with the three different values of the coupling constant $g_{K^*N\Lambda^*}$. K^*-exchange plays a significant role in describing the Λ^* production off the neutron. Furthermore, the total cross section is proportional to $\sim(E_\gamma - E_{\rm th})^{1/2}$ by K^*-exchange. When K^* exchange is switched off, i.e. $g_{K^*N\Lambda^*} = 0$, the total cross section is strongly suppressed and the p-wave is found to be dominant, so that its energy dependence is changed to be proportional to $(E_\gamma - E_{\rm th})^{3/2}$ as shown in Fig. 7.

In the right panel of Fig. 7, $d\sigma/dt$ is drawn at $E_\gamma = 3.8$ GeV. It is natural that the t-dependence for the neutron target be very different from that for the proton, since dominant diagrams are different for each case.

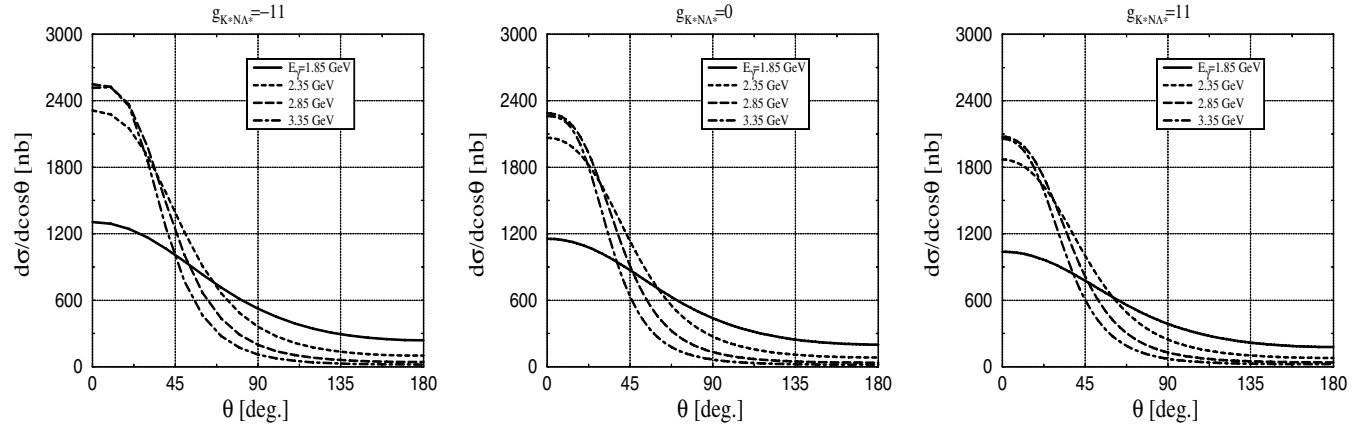

FIG. 6. The differential cross sections for the proton target with the form factor F_1. Several photon energies are taken into account. We choose $(\kappa_{\Lambda^*}, X) = (0, 0)$.

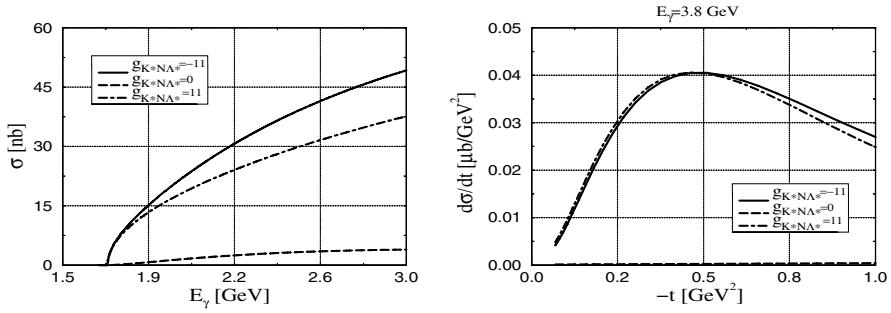

FIG. 7. In the left panel, the total cross sections are depicted for the neutron target with the form factor F_1, while in the right panel the t-dependence is drawn at $E_\gamma = 3.8$ GeV. We choose $(\kappa_{\Lambda^*}, X) = (0, 0)$ and three different values of the coupling constants, i.e. $g_{K^*N\Lambda^*} = 0$ and ± 11.

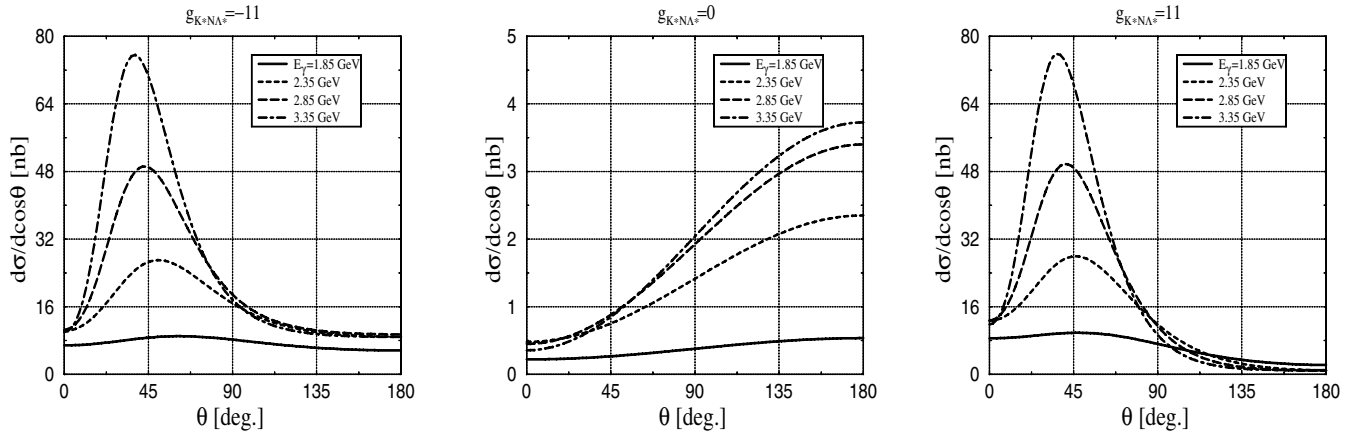

FIG. 8. The differential cross sections for the neutron target with the form factor F_1. Several photon energies are taken into account. We choose $(\kappa_{\Lambda^*}, X) = (0, 0)$.

Figure 8 presents the differential cross sections for the neutron target with three different values of $g_{K^*N\Lambda^*}$. While the sign of the coupling constant does not change the results, its absolute value seems to be of great importance. For example, K^*-exchange being included with $g_{K^*N\Lambda^*} = \pm 11$, the differential cross sections are enhanced around 45°. Note that the sign of $g_{K^*N\Lambda^*}$ is not important. The bump around 45° is a typical behavior when we introduce the form factor like F_1 in the t-channel.

C. $\gamma N \to K\Lambda^*$ with the form factor F_2

When the form factor F_2 defined in Eq. (9) is used, the results turn out to be quite different from those with F_1. We determine the cutoff mass $\Lambda_2 = 650$ MeV by fitting the total cross section to the experimental data around $E_\gamma \sim 3$ GeV from Ref. [4]. As in the previous case, we fix two parameters $(\kappa_{\Lambda^*}, X) = (0, 0)$, so that the relevant contributions are from the s-, t-, c-channels and K^*-exchange.

In the left panel of Fig. 9, we show the total cross sections as functions of the incident photon energy E_γ for the proton target. While the energy dependence looks similar to that with the form factor F_1 as drawn in Fig. 4, the magnitude is quite larger than that. Moreover, the energy dependence of K^* exchange is changed by replacing the form factor F_1 by the F_2 as shown in Fig. 9. This can be understood by comparing the F_2 with the F_1, defined in Eqs. (8) and (9), respectively. While the form factor F_2 has an overall energy dependence, the F_1 does not.

We plot the t-dependence for the proton target in the right panel of Fig. 9, using the form factor F_2. The curves show quite different t-dependence from those with the F_1 (Fig. 5). Thus, the results deviate from the data when using the F_2, though we have obtained the reasonable size and energy dependence of the total cross sections as shown in the left panel of Fig. 9.

In Fig. 10, we depict the differential cross sections for the proton target at $E_\gamma = 3.8$ GeV with the form factor F_2. Compared to those with F_1 drawn in Fig. 6, they look very different. When the F_2 is employed, the backward peak is enhanced as the energy increases, whereas the F_1 does the forward one. These behaviors arise from the different angular dependences of the form factors. Note that the F_1 suppresses the differential cross sections at backward

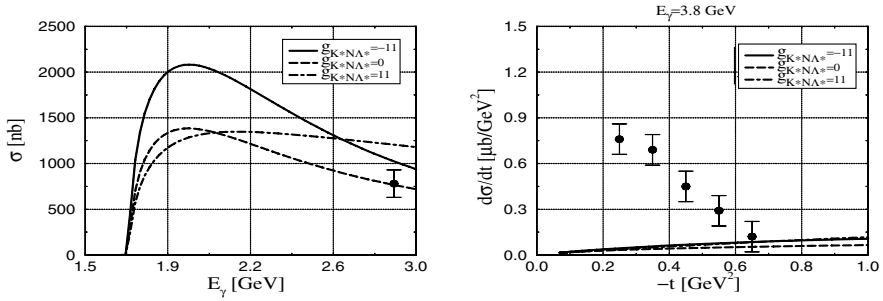

FIG. 9. In the left panel, the total cross sections are depicted for the proton target with the form factor F_1, while in the right panel the t-dependence is drawn for the proton target at $E_\gamma = 3.8$ GeV. We choose $(\kappa_{\Lambda^*}, X) = (0, 0)$ and three different values of the coupling constants, i.e. $g_{K^*N\Lambda^*} = 0$ and ± 11.

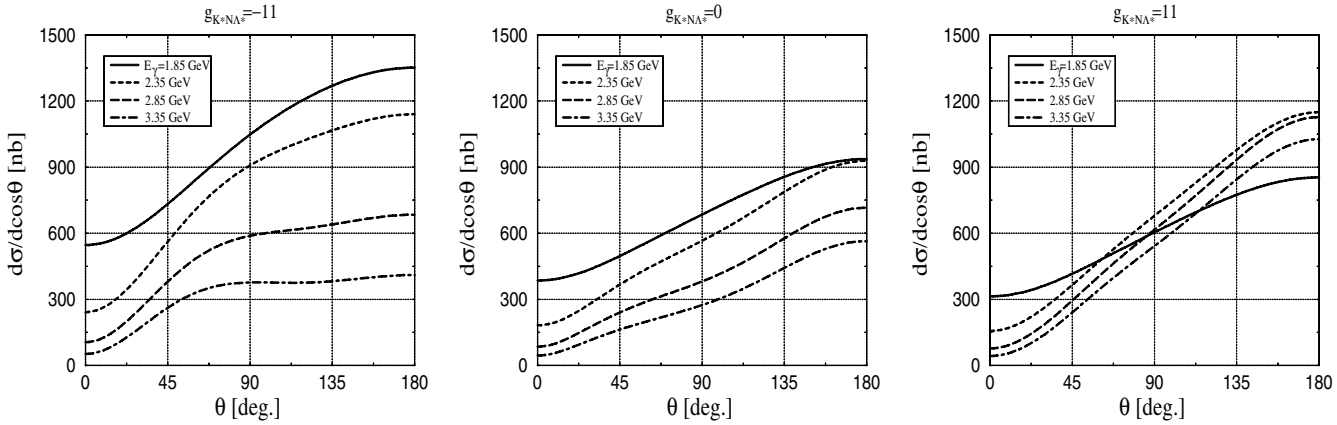

FIG. 10. The differential cross sections for the proton target with the form factor F_2. Several photon energies are taken into account. We choose $(\kappa_{\Lambda^*}, X) = (0, 0)$.

angles, while the F_2 does not influence the angular distribution. The ambiguity arising from the form factors is one of the sources of theoretical uncertainties in describing hadronic reactions, in particular, at the higher energy region. By fitting the results to the experimental data, we can reduce those uncertainties.

Finally, we discuss the total cross sections for the neutron target. The left panel of Fig. 11 draws them and the right one the t-dependence, and Fig. 12 the angular distribution. In contrast with those with the form factor F_1, the sign and absolute values of $g_{K^*N\Lambda^*}$ do not influence much the total cross sections, since the form factor F_2 suppresses all channels on the same footing. Thus, the magnitudes of the total cross sections are rather similar to those of the proton target. As shown in Fig. 12, the backward bump is even more enhanced as the energy increases in comparison with those for the proton target. However, as the energy increases, the size of the bump is more or less saturated.

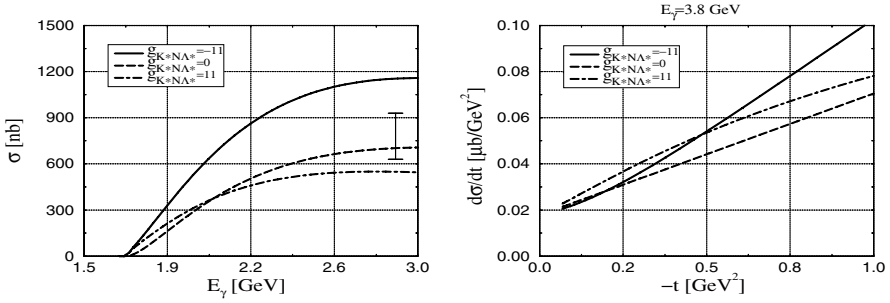

FIG. 11. In the left panel, the total cross sections are depicted for the neutron target with the form factor F_1, while in the right panel the t-dependence is drawn at $E_\gamma = 3.8$ GeV. We choose $(\kappa_{\Lambda^*}, X) = (0, 0)$ and three different values of the coupling constants, i.e. $g_{K^*N\Lambda^*} = 0$ and ± 11.

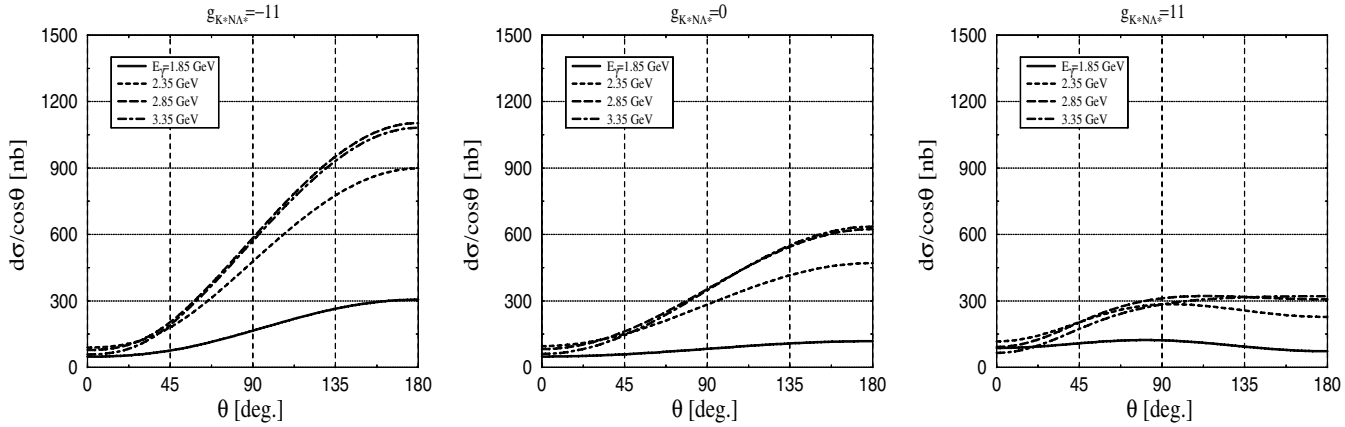

FIG. 12. The differential cross sections for the neutron target with the form factor F_2. Several photon energies are taken into account. We choose $(\kappa_{\Lambda^*}, X) = (0, 0)$.

D. Comparison to the $\gamma N \to \bar{K}\Theta^+$ reaction

Recently, the LEPS collaboration has performed an experiment searching for the Θ^+ in the two-body process $\gamma d \to \Lambda^* \Theta^+$. Since, the statistics for the Λ^* photoproduction is much higher than that of the Θ^+, the reaction can be used to extract information on the production mechanism of the Θ^+ by comparing it with the Λ^* photoproduction. In the previous studies [21,22] and in the present work, we have observed that the $\gamma n \to K^- \Theta^+$ and $\gamma p \to K^+ \Lambda^*$ reactions are less parameter-dependent. Note that both are charge-exchange processes. We first consider the positive-parity Θ^+ with spin-$1/2^+$. We apply the gauge-invariant from-factor F_1 with the cutoff mass $\Lambda = 750$ to both reactions. The coupling constants for the Θ^+ are taken to be $g_{KN\Theta} = 1.0$ [19] and $g_{K^*N\Theta} = +\sqrt{3} g_{KN\Theta}$ [23]. The former corresponds to the decay width $\Gamma_{\Theta \to KN} \sim 1$ MeV. Then we find that the total cross section for the Θ^+ photoproduction is $2 \sim 3$ nb in average up to $E_\gamma = 3.0$ GeV. The angular dependence shows a bump around 50° at $E_\gamma = 1.8$ GeV. The bump moves closer to $\theta = 0$ as the photon energy increases. Since the angular dependence of the Λ^* photoproduction is enhanced in the forward direction as the photon energy increases (see Fig. 6), the angular dependences for both reactions are qualitatively similar each other. Considering the angular dependences of the two reactions and the present total cross section of the Λ^* photoproduction (see Fig. 4), we find the ratio R of the total cross sections of these two reactions as follows:

$$R = \frac{\sigma_{\gamma n \to K^- \Theta^+}}{\sigma_{\gamma p \to K^+ \Lambda^*}} = \frac{1}{300} \sim \frac{1}{400}. \tag{10}$$

As for the negative-parity Θ^+, the values of R will be decreased approximately by a factor of 10 [21]. We verify that even if we use the form factor F_2, the situation does not change much.

IV. THE ROLE OF K^*-EXCHANGE

In Ref. [4] of the Daresbury experiment, it was argued that the Λ^* photoproduction was dominated by vector K^*-exchange (u-channel) rather than pseudoscalar K-exchange (t-channel) by analyzing the decay amplitude in the t-channel in the helicity basis of the Λ^*. If the helicity of the Λ^* is $S_z = \pm 3/2$, the decay of $\Lambda^* \to K^- p$ is explained by $\sin^2\theta$ in which θ is the angle between the two kaons in the helicity basis (see Ref. [5] for details). On the other hand, $1/3 + \cos^2\theta$ characterizes the angular dependence of the decay of the $S_z = \pm 1/2$ state. Therefore, taking into account the ratio of these two helicity amplitudes, one could extract information as to which meson would dominate. In Ref. [4], it was shown that the ratio of $(S_z = \pm 1/2)/(S_z = \pm 3/2)$ was nearly zero. Thus, it was suggested that the Λ^* photoproduction was dominated by the u-channel.

In Fig. 13, we plot the t-dependence for each helicity using the form factor F_1 with three different values for the coupling constants $g_{K^*N\Lambda^*}$. Here, we do not discuss the case of using the form factor F_2, since this form factor fails to reproduce the experimental data of Ref. [4]. We choose $E_\gamma = 3.8$ GeV as done previously. In Fig. 13, we observe that the $S_z = \pm 3/2$ contribution is dominant especially in the region $-t \lesssim 0.2$ GeV^{-2}. There is also a small contribution from the $S_z = \pm 1/2$. However, we find that even without the u-channel ($g_{K^*N\Lambda^*} = 0$) the $S_z = \pm 3/2$ does not become zero. Therefore, the $S_z = \pm 3/2$ contribution comes not only from the u-channel but also from the other channels.

In order to see this situation more carefully, we pick up three important channels, the c-, t- and u-channels, and plot the t-dependence for each helicity in Fig. 14. One can see that the $S_z = \pm 1/2$ contribution is larger than that of the $S_z = \pm 3/2$ for pseudoscalar K-exchange (t-channel), and vice versa for the u-channel. We also observe that the c-channel has sizable contributions to both $S_z = \pm 1/2$ and $S_z = \pm 3/2$ amplitudes. From these observations, our

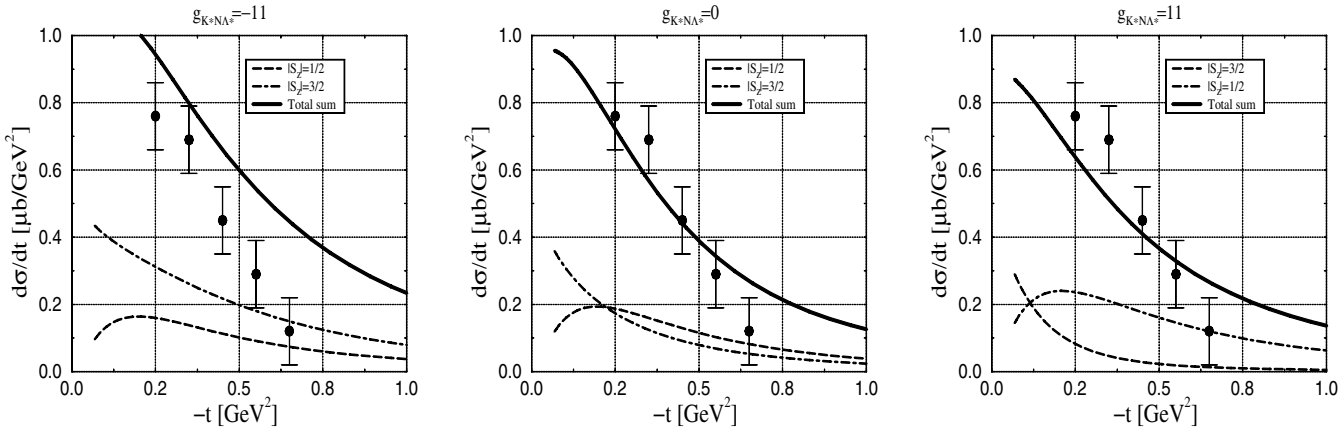

FIG. 13. The t-dependence for each helicity of the Λ^* in the final state. We change the coupling constant $g_{K^*N\Lambda^*}$. We choose $(\kappa_{\Lambda^*}, X) = (0, 0)$.

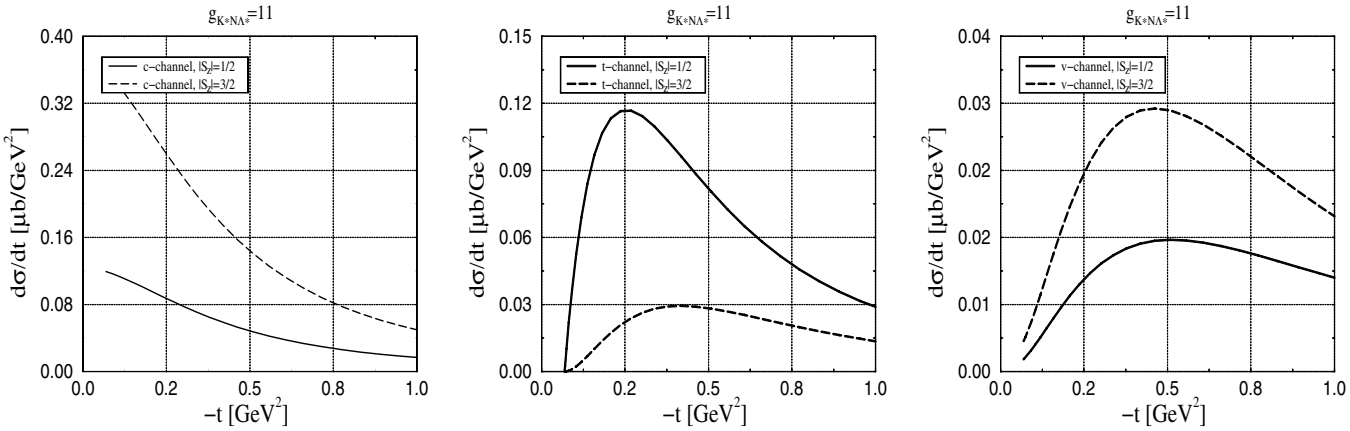

FIG. 14. The t-dependence for the two helicities $S_z = \pm 1/2$ and $S_z = \pm 3/2$ for the c-, t- and υ-channels.

model calculation using the form factor F_1 indicates that the $S_z = \pm 3/2$ contribution is significant as shown in Ref. [4]. However, most of the $S_z = \pm 3/2$ contribution comes from the c-channel, not from the υ-channel as suggested in Ref. [4]. We also find that the sizable $S_z = \pm 1/2$ contributions are produced from the c- and t-channels. Therefore, in order to reproduce a nearly zero value of the ratio of $(S_z = \pm 1/2)/(S_z = \pm 3/2)$ [4], we need a more suppression factor in the t-channel, which is the major source of the $S_z = \pm 1/2$ contribution in the Λ^* photoproduction.

V. SUMMARY AND CONCLUSIONS

In the present work, we investigated the $\Lambda^*(1520, 3/2^-)$ photoproduction via the $\gamma N \to K\Lambda^*$ reaction. We employed the Rarita-Schwinger formalism for describing the spin-3/2 particle for a relativistic description. Taking into account the effective Lagrangians for the Born diagrams, we constructed the invariant amplitudes for the reaction. The model parameters such as the anomalous magnetic moment of Λ^*, κ_{Λ^*} and the off-shell parameter X were tested for their sensitivity. We found that the parameter dependence turned out to be rather weak in the low-energy region ($E_\gamma \lesssim 3$ GeV). Furthermore, the quark-model calculation indicated that κ_{Λ^*} was relatively small and can be ignored. Therefore, we set these two unknown parameters, κ_{Λ^*} and X, equal to zero for the numerical calculations. The coupling constant $g_{K^*N\Lambda^*}$ was taken to be 0 and ± 11, since the quark model showed that $g_{K^*N\Lambda^*}$ was in the same order as $g_{KN\Lambda^*}$. In order to check the theoretical ambiguities, we used the gauge-invariant four-dimensional form factor F_1 and the three-dimensional one F_2.

We performed the numerical calculations for the $\gamma p \to K^+\Lambda^*$ and $\gamma n \to K^0\Lambda^*$ separately for the two different types of the form factors. As for the total cross sections for the proton target, these two different form factors gave similar results in magnitude and energy dependence, whereas quite different behaviors were found for the neutron target. The total cross sections for the neutron target using the form factor F_1 are much smaller than those with the F_2. However, since the F_2 failed to reproduce the existing experimental data of the momentum transfer

TABLE I. Summary of the results.

Form factor	F_1		F_2	
Reactions	$\gamma p \to K^+\Lambda^*$	$\gamma n \to K^0\Lambda^*$	$\gamma p \to K^+\Lambda^*$	$\gamma n \to K^0\Lambda^*$
σ	$\sim$900 *nb*	$\sim$30 *nb*	$\sim$1200 *nb*	$\sim$700 *nb*
$d\sigma/d(\cos\theta)$	Forward peak	Peak at $\sim$45°	Backward peak	Backward peak
$d\sigma/dt$	Good	No data	Bad	No data

t-dependence for the proton target, it can be ruled out. The F_1 describes it qualitatively well. We summarize the whole numerical results briefly in Table I.

When we compare the present results to those for the Θ^+ photoproduction, the ratio of the total cross sections for these two photo-reactions turns out to be $1/300 \sim 1/400$ for the positive-parity Θ^+ baryon. As for the negative parity Θ^+, it is suppressed by a factor of about ten [21,22]. We confirm that this ratio is less dependent on the model parameters for the charge-exchange reactions such as ($\gamma n \to K^-\Theta^+$, $\gamma p \to K^+\Lambda^*$). As for the helicity dependence, though the contribution of the $S_z = \pm 3/2$ was dominant, it was not directly related to the K^*-exchange dominance as suggested in Ref. [4].

ACKNOWLEDGMENTS

We thank T. Nakano, H. Toki, A. Titov, E. Oset, and M. J. Vicente Vacas for fruitful discussions and comments. The work of S. I. N. has been supported by the Ministry of Education, Culture, Science and Technology of Japan. The works of A. H. and S. I. N. are partially supported by the collaboration program of RCNP, Osaka Univ., Japan and IFIC, Valencia Univ., Spain. The work of A. H. is also supported in part by the Grant for Scientific Research ((C) No.16540252) from the Education, Culture, Science and Technology of Japan. The works of H. Ch. K. and S. I. N. are supported by the Korean Research Foundation (KRF-2003-070-C00015).

APPENDIX: RARITA-SCHWINGER VECTOR-SPINOR

We can write the RS vector-spinors according to their spin states as follows:

$$
\begin{aligned}
u^\mu\left(p_2,\frac{3}{2}\right) &= e_+^\mu(p_2)u\left(p_2,\frac{1}{2}\right),\\
u^\mu\left(p_2,\frac{1}{2}\right) &= \sqrt{\frac{2}{3}}e_0^\mu(p_2)u\left(p_2,\frac{1}{2}\right)+\sqrt{\frac{1}{3}}e_+^\mu(p_2)u\left(p_2,-\frac{1}{2}\right),\\
u^\mu\left(p_2,-\frac{1}{2}\right) &= \sqrt{\frac{1}{3}}e_-^\mu(p_2)u\left(p_2,\frac{1}{2}\right)+\sqrt{\frac{2}{3}}e_0^\mu(p_2)u\left(p_2,-\frac{1}{2}\right),\\
u^\mu\left(p_2,-\frac{3}{2}\right) &= e_-^\mu(p_2)u\left(p_2,-\frac{1}{2}\right).
\end{aligned}
\tag{A1}
$$

Here, we employ the basis four-vectors, e_λ^μ which are written by

$$
\begin{aligned}
&e_\lambda^\mu(p_2) = \left(\frac{\hat{e}_\lambda\cdot\vec{p}_2}{M_B},\quad \hat{e}_\lambda+\frac{\vec{p}_2(\hat{e}_\lambda\cdot\vec{p}_2)}{M_B(p_2^0+M_B)}\right)\\
&\text{with } \hat{e}_+ = -\frac{1}{\sqrt{2}}(1,i,0),\quad \hat{e}_0=(0,0,1)\\
&\text{and } \hat{e}_- = \frac{1}{\sqrt{2}}(1,-i,0).
\end{aligned}
\tag{A2}
$$

[1] T. Nakano *et al.* (LEPS Collaboration), Phys. Rev. Lett. **91**, 012002 (2003); V. V. Barmin *et al.* (DIANA Collaboration), Phys. At. Nucl. **66**, 1715 (2003); [Yad. Fiz. **66**, 1763 (2003)]; S. Stepanyan *et al.* (CLAS Collaboration), Phys. Rev. Lett. **91**, 252001 (2003); **92**, 049902 (2004); Phys. Rev. Lett. **92**, 032001 (2004); J. Barth *et al.* (SAPHIR Collaboration), Phys. Lett. B (to be published); A. Airapetian *et al.* (HERMES Collaboration), Phys. Lett. B **585**, 213 (2004).

[2] T. Nakano, talk in the international workshop Chiral 05, RIKEN, February (2005).

[3] A. Boyarski, R. E. Diebold, S. D. Ecklund, G. E. Fischer, Y. Murata, B. Richter, and M. Sands, Phys. Lett. B **34**, 547 (1971).

[4] D. P. Barber *et al.*, Z. Phys. C **7**, 17 (1980).

[5] S. P. Barrow *et al.* (Clas Collaboration), Phys. Rev. C **64**, 044601 (2001).

[6] K. Ohta, Phys. Rev. C **40**, 1335 (1989).

[7] H. Haberzettl, C. Bennhold, T. Mart, and T. Feuster, Phys. Rev. C **58**, 40 (1998).

[8] R. M. Davidson and R. Workman, Phys. Rev. C (to be published).

[9] W. Rarita and J. S. Schwinger, Phys. Rev. **60**, 61 (1941).

[10] B. J. Read, Nucl. Phys. B **52**, 565 (1973).

[11] K. Johnson and E. C. G. Sudarshan, Annals Phys. **13**, 126

(1961).
[12] G. Velo and D. Zwanziger, Phys. Rev. **188**, 2218 (1969).
[13] V. Pascalutsa, Phys. Rev. D **58**, 096002 (1998).
[14] G. Hoehler, H. P. Jakob, and R. Strauss, Nucl. Phys. **B39**, 237 (1972).
[15] L. M. Nath, B. Etemadi, and J. D. Kimel, Phys. Rev. D **3**, 2153 (1971).
[16] C. R. Hagen, Phys. Rev. D **4**, 2204 (1971).
[17] R. Machleidt, K. Holinde, and C. Elster, Phys. Rep. **149**, 1 (1987).
[18] M. Gourdin, Nuovo Cimento **36**, 129 (1965); **40A**, 225 (1965).
[19] S. Eidelman *et al.* (Particle Data Group), Phys. Lett. B **592**, 1 (2004).
[20] S. I. Nam, A. Hosaka, and H.-Ch. Kim, hep-ph/0502143.
[21] S. I. Nam, A. Hosaka, and H.-Ch. Kim, Phys. Lett. B **579**, 43 (2004).
[22] S. I. Nam, A. Hosaka, and H.-Ch. Kim, Phys. Rev. D (to be published).
[23] F. E. Close and J. J. Dudek, Phys. Lett. B **586**, 75 (2004).